Suh, J.; Victoria-Hernandez, J.; Letzig, D.; Golle, R.; Volk, W.:

Enhanced mechanical behavior and reduced mechanical anisotropy of AZ31 Mg alloy sheet processed by ECAP

In: Materials Science and Engineering A (2015) Elsevier

DOI: 10.1016/j.msea.2015.09.058

Enhanced mechanical behavior and reduced mechanical anisotropy of AZ31 Mg alloy sheet processed by ECAP

Joungsik Suh[a], Jose Victoria-Hernandez[b], Dietmar Letzig[b], Roland Golle[a], Wolfram Volk[a,*]

[a] Institute of Metal Forming and Casting, Technische Universität München, Walther-Meißner-Str. 4, Garching, D-85748, Germany

[b] Magnesium Innovation Centre, Helmholtz-Zentrum Geesthacht, Max-Planck-Str. 1, Geesthacht, D-21502, Germany

*Corresponding author Tel.: +49 89 289 13790; Fax.: +49 89 289 13738

E-mail address: wolfram.volk@utg.de (W. Volk)

Abstract

AZ31 Mg alloy sheets were processed by equal channel angular pressing (ECAP) at 225 °C with a channel angle of 110° regarding a new processing route. In consideration of mechanical anisotropy of Mg sheets, the sheet was processed by ECAP along the rolling direction in the first pass. Subsequently, it was processed along the transverse direction by 90° rotation around the normal direction in the sheet plane. This shear deformation led to grain refinement and developed a texture with tilted basal planes towards the pressing direction. The new presented processing route, which is denoted as route D, reduced mechanical anisotropy and enhanced hardening behavior. As a result, the ECAPed AZ31 sheet on route D exhibited an almost isotropic hardening at room temperature with improved ductility.

Keywords: ECAP; Magnesium alloy; Texture; Anisotropy; Work hardening

1. Introduction

Mg and its alloys with hexagonal close-packed lattice exhibit the limited number of active slip systems at room temperature [1]. Typical wrought Mg alloys develop strong basal texture during rolling [2]. This texture with a preferred orientation, where the basal planes are parallel to the sheet plane, causes mechanical anisotropy and poor formability at room temperature [3]. The limited formability of Mg alloy sheets is one of the main reasons hindering industrial applications. Grain refinement and texture modification can improve the forming characteristics of Mg alloy sheets [4].

Equal channel angular pressing (ECAP) provides possibilities for producing semi-finished materials with fine grains and unique textures [5,6]. There are extensive studies on the processing of Mg alloys by ECAP regarding the effect of the processing temperature [6,7], channel angle [8-10] and processing route [11-13]. They reported that the grain refinement and texture change induced by ECAP lead to high improvement of tensile properties. However, the existing studies on ECAP are limited to bulk materials, e.g. extruded bars.

For the application of ECAP to Mg alloy sheets, it is necessary to investigate systematically the process parameters. In this regard, Suh et al. [14] investigated the microstructure and resulting mechanical behavior at room temperature of AZ31 sheets, which were processed by ECAP at 175, 200 and 225 °C with a channel angle (Φ) of 130°. Grain structure becomes more homogeneous and finer with increasing processing temperature. Particularly, shear deformation induced by ECAP leads to a broad angular distribution of the basal planes from the normal direction (ND) towards the pressing direction (PD), which was in that study parallel to the rolling direction (RD). Consequently, the uniform elongation (ε_u) in the RD of AZ31 sheet, which was processed by ECAP at 225 °C, was improved by 31% compared to the rolled sample.

ECAP offers the possibility of multiple repetitions, so that further significant changes in texture and grain structure can be achieved due to a change of the sample orientation with respect to the shear direction, i.e. processing route. In this study, AZ31 sheets were processed by ECAP at 225 °C with Φ = 110° regarding the strain path change. Considering mechanical anisotropy of Mg sheets, the new presented processing route is denoted as route D. On route D, the PD is parallel to the RD in the first pass and to the TD in the second pass by 90° rotation around the ND. The present study aims to investigate the effect of the modified processing route on the microstructure and mechanical behavior at room temperature of equal-channel angularly processed (ECAPed) AZ31 sheets.

2. Experimental procedure

Hot-rolled AZ31 Mg alloy (3Al-1Zn-0.3Mn-Mg Bal. wt.%) sheets with a thickness of 1.8 mm were used in this work. After hot rolling, a recrystallization annealing was performed at 350 °C for 0.5 h. An ECAP test tool was designed and manufactured for imposing shear strain on sheets as presented in Fig. 1a [14]. In the open position, a sheet with dimensions of 200 × 200 × 1.8 mm^3 was laterally inserted between the tool elements. During closing of the blank holder plate with a press speed of 5 mm/s, the sheet was locally heated by the both channel parts, which were pre-heated at 225 °C using two cartridge heaters. Subsequently, it was pressed through the channel part with Φ = 110°. The analytically effective strain per pass with Φ = 110° is ~0.8 [15]. On the new presented route D, the shear strain is imposed on the RD and subsequently on the TD with 90° rotation in the sheet plane (Fig. 1b). After each pass, the ECAPed sheets were hot-leveled at 200 °C for 0.5 h with a pressure of 7.3 kPa, to achieve a homogeneous microstructure and completely flat sheets.

The microstructures of the rolled and ECAPed sheets were analyzed by electron backscatter diffraction (EBSD) using a field emission gun scanning electron microscope (Zeiss^{TM}, Ultra 55). Longitudinal sections of the samples were polished electrochemically using a Struers^{TM} AC2 solution at 16 V for 80 s at -25 °C. EBSD measurements were implemented at an accelerating voltage of 15 kV and a step size of 0.3 µm over an area of 150 x 300 µm^2.

Quantitative texture measurements were implemented with a Panalytical^{TM} X-ray diffractometer (XRD) in reflection geometry using Cu-Kα radiation. Six pole figures, (0001), (10-10), (10-11), (10-12), (10-13) and (11-20), were measured up to a tilt angle of 70°. The data were used to calculate the orientation distribution function and recalculate pole figures. In this study, (0001) pole figure represents the global texture of the rolled and ECAPed sheets.

Tensile specimens at the angles of 0°, 45° and 90° to the RD were prepared according to DIN 50125 H 12.5 × 50. Tensile tests were performed at room temperature with a quasi-static strain rate of 1.0×10^{-3} s^{-1} using a Zwick^{TM} Typ 1484/DUPS-M testing machine. The Lankford coefficient (r-value) was calculated at 10% engineering strain in each tensile direction and is designated as r_{10}. The strain hardening exponents (n-value) were calculated by power law regression over the strain range from 10 to 15%.

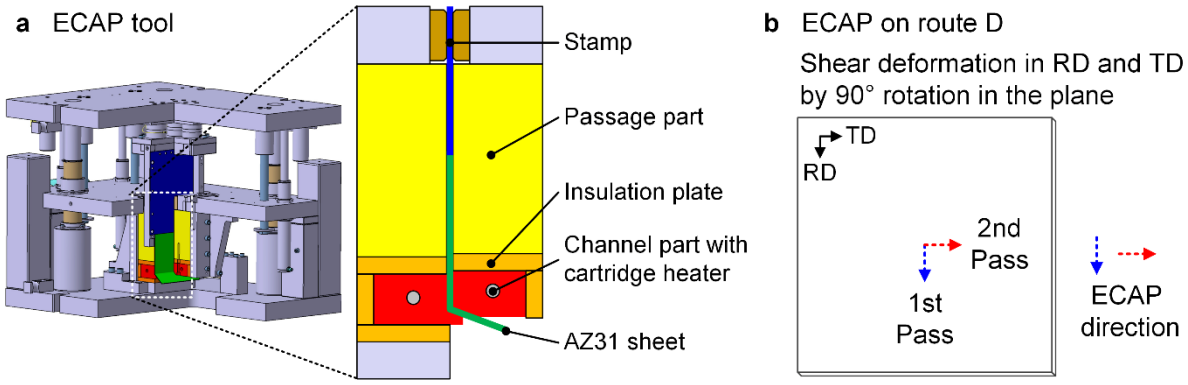

Fig. 1. Schematic description of ECAP tool and route D: (a) ECAP tool, (b) route D.

3. Results and discussion

3.1. Microstructure and texture evolution

Fig. 2 shows the microstructures of the rolled and ECAPed AZ31 sheets using EBSD inverse pole figure (IPF) map. The microstructure of the rolled sheet exhibits a twin-free equiaxed grain structure. It can be clearly observed that ECAP process has a significant effect on grain refinement. In comparison of the as-rolled sample, the average grain size (d) is refined from 14 to 8.4 µm after the single ECAP pass. The microstructure develops with a high fraction of serrated grain boundaries and fine grains in Fig. 2b. This microstructural feature is one of the typical characteristics of Mg alloys that underwent dynamic recrystallization [16]. This results from continuous production and absorption of dislocation in low angle grain boundaries, as well as progressive transformation to high angle grain boundaries [17]. New recrystallized grains surround the original grain boundaries, resulting in necklace structure [17]. Despite two ECAP passes on route D, the average grain size is not refined further and amounts to 10.5 µm (Fig. 2c). However, a more homogenous microstructure with equiaxed grains develops through route D compared to the ECAPed sample in a single pass. The shear deformation after the second ECAP pass may consume the serrated boundaries and small grains of the first ECAP pass, and hence build new grains. Furthermore, the IPF map of the rolled sheet shows that most grains have

(0001) axis parallel to the ND. In contrast, many grains of the ECAPed sheets exhibit other different directions apart from the ND. It is evident that the preferred orientation of the rolled sheet is weakened and randomized by ECAP.

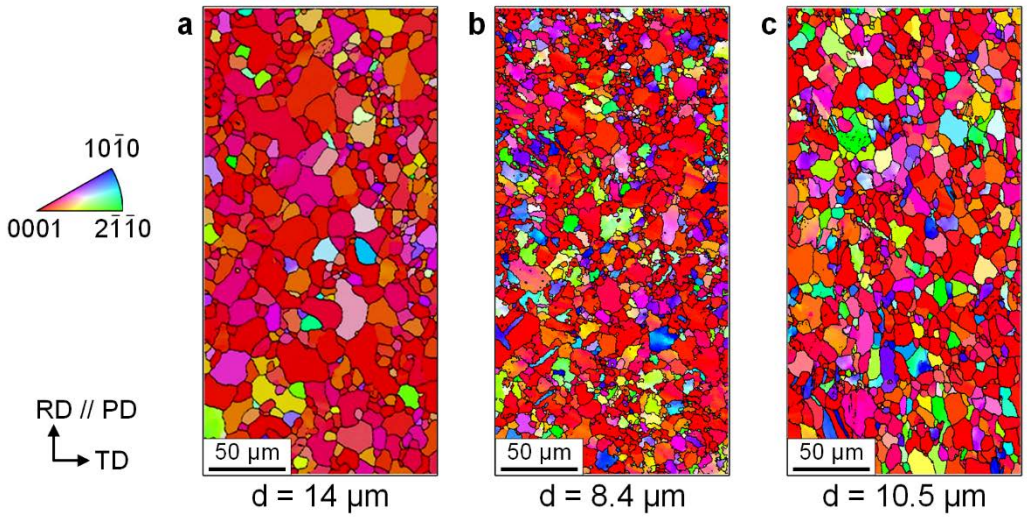

Fig. 2. IPF maps of rolled and ECAPed AZ31 sheets regarding strain path: (a) as-rolled condition, (b) single pass, (c) route D.

Fig. 3 presents the global texture of the rolled and ECAPed sheets in the form of (0001) pole figure from the XRD measurements. Even if there is no distinct difference in the maximum pole intensity (I_{max}), the basal planes are distributed differently between the rolled and ECAPed sheets. Compared to the rolled sheet, the basal planes of the ECAPed sheets are spread broadly from the ND to the PD. In the single pass, there is a broad intensity spread of the basal planes along the RD with ~5° inclination of the I_{max} (Fig. 3b). A texture component is developed, which is tilted by ~80° towards the RD. It originates from the activation of {10-12} <10-11> twins, which can reorient the c-axis ~86° away of the original direction [18]. This twinning mode is the most commonly and easily activated twin in Mg [19]. On the other hand, the texture on route D is slightly strengthened and the texture component in the RD, which was generated in the first pass, weakens. Instead, the new component

develops visibly along the TD. The I_{max} in the RD and TD is inclined comparably by ~5°. Especially, the basal planes are tilted by ~15° at 45° to the RD. It certainly suggests that this unique texture evolution has a distinct influence on the mechanical anisotropy.

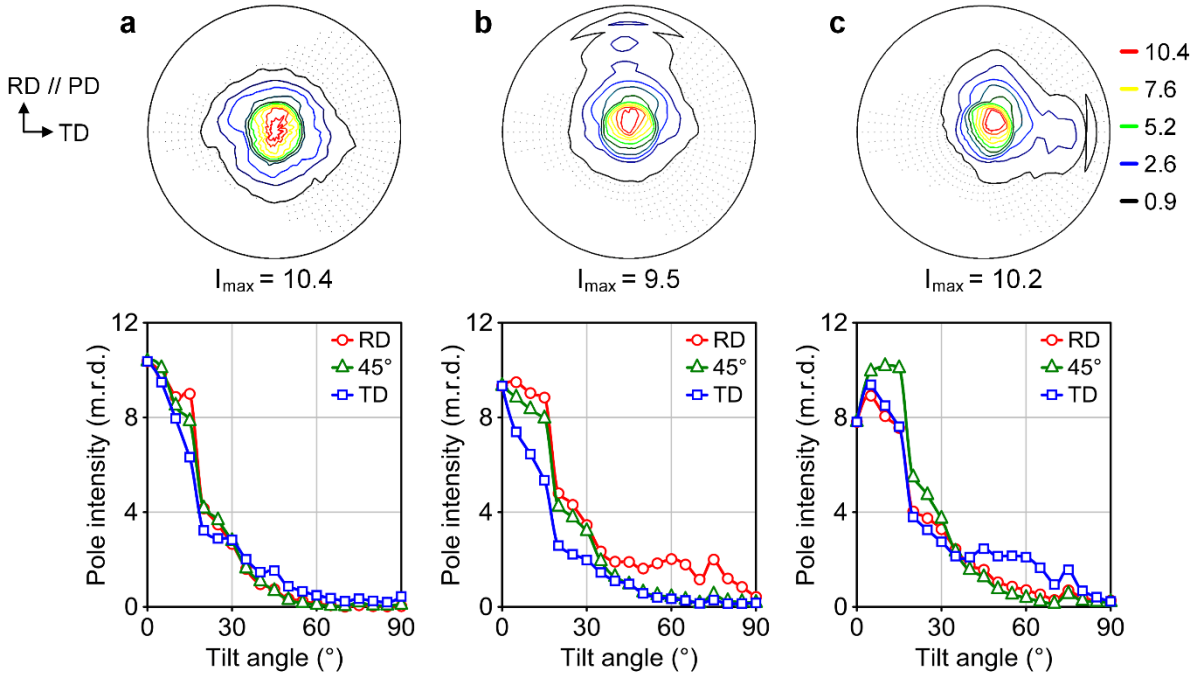

Fig. 3. (0001) pole figures and corresponding intensity profiles of rolled and ECAPed AZ31 sheets: (a) as-rolled condition, (b) single pass, (c) route D.

Fig. 4 shows the EBSD analysis of the Schmid factor for basal <a> slip (m_{basal}) in tension along the RD and TD. The Schmid factor is a geometrical value that indicates the feasibility to activate a certain slip mode regarding the loading direction. Since basal <a> slip is the easiest deformation mode at room temperature, the distribution of Schmid factor is useful to analyze the effect of the reorientation of the basal planes on the activation of basal <a> slip. According to the above-presented IPF maps (refer to Fig. 2) and the definition of the Schmid factor, the m_{basal} should be low for the as-rolled condition. The reason is that the c-axis of most grains is parallel to the ND of the sheet, and thus the basal planes are mostly parallel to the loading direction. By

contrast, ECAPed sheets can exhibit high m_{basal} due to the texture with an inclined c-axis towards the PD.

Fig. 4a and b present the distribution of the m_{basal} in tension along the RD or the TD, respectively. It is remarkably evident that ECAP has a considerable effect on the activation of basal <a> slip along the PD. The reason is that the shear deformation induced by ECAP increases the fraction of grains with high m_{basal} of 0.4. As a result, the single pass has the highest value in the RD and route D exhibits the highest one in the TD. For the rolled sheet, the m_{basal} is lower in both directions.

Another important feature is that high fractions of twins are observed in the ECAPed microstructure. Some examples are marked inside the dashed white squares and in the close up of Fig. 4c. Most of twins originate from {10-12} tensile twinning. This twinning mode is preferred, when applying tension parallel to the c-axis or contraction perpendicular to the c-axis [20]. As a characteristic feature, twinning can rotate unfavorably oriented crystals to favorable direction for dislocation slip [21]. Consequently, {10-12} tensile twinning can increase the Schmid factor and contribute to further activation of basal <a> slip. Besides, the texture of the ECAPed sheet with the inclined c-axis can experience further the activation of {10-12} tension twins, because tensile twinning accommodates tension along the c-axis [14].

Table 1 summarizes the calculated Schmid factors for basal <a> slip, prismatic <a> slip and pyramidal <c+a> slip. According to the Schmid's law [22], high average m_{basal} of the ECAPed sheets can lead to a considerable decrease of yield strength (YS) in each tensile direction. Moreover, it is found that the rotation of the basal planes during ECAP has an influence on the activity of prismatic and pyramidal slip. As will be discussed in section 3.3, the reduction of the Schmid factors, especially those of prismatic slip, have a significant effect on work hardening behavior of the ECAPed samples.

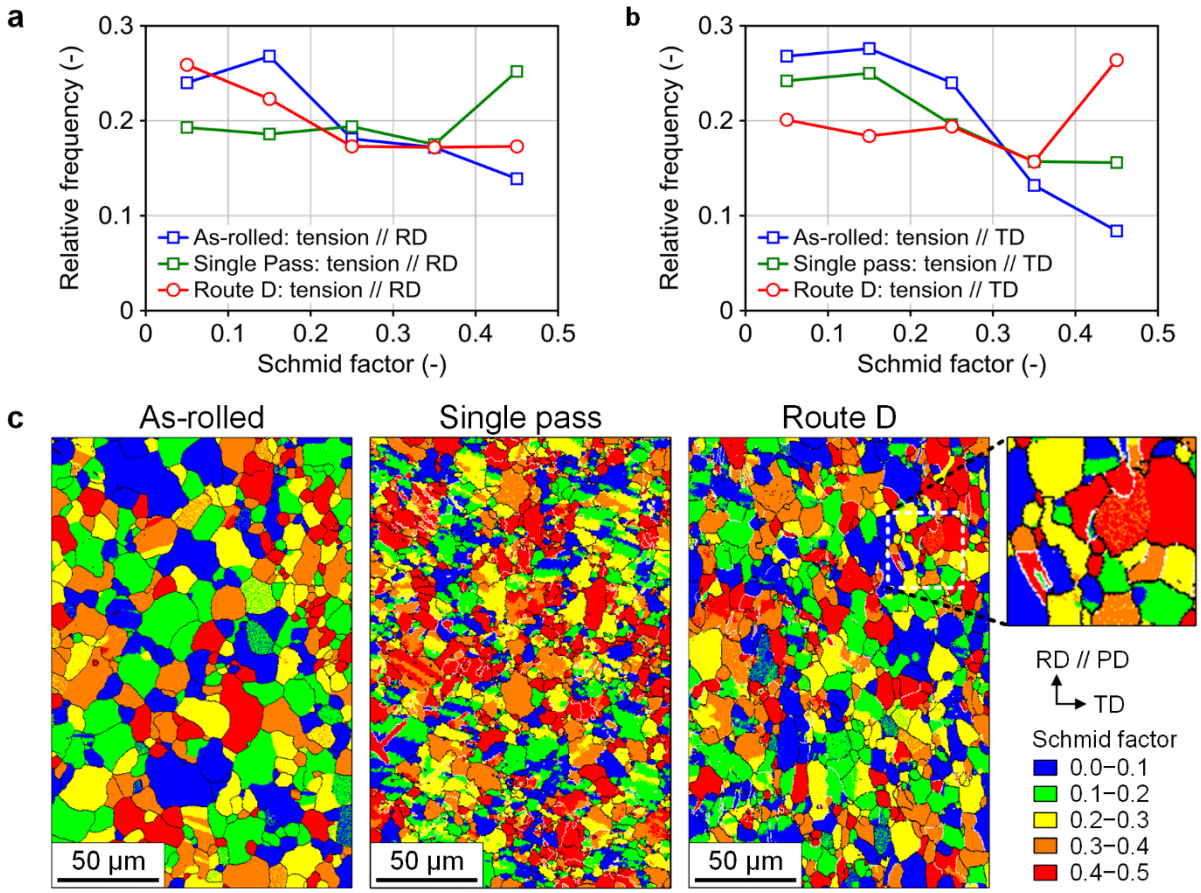

Fig. 4. Analysis of Schmid factor of basal <a> slip for rolled and ECAPed AZ31 sheets: (a) Schmid factor distribution in terms of relative frequency (tension parallel to RD), (b) Schmid factor distribution (tension parallel to TD), (c) Schmid factor maps when applying a virtual tension parallel to RD (black line: grain boundary, white line: twin boundary).

Table 1 Average Schmid factors for slip systems of rolled and ECAPed AZ31 sheets when applying a virtual tension along RD or TD.

	As-rolled		Single pass		Route D	
	RD	TD	RD	TD	RD	TD
Basal <a> slip (0001) <11-20>	0.220	0.199	0.261	0.224	0.228	0.260
Prismatic <a> slip (1-100) <11-20>	0.431	0.425	0.363	0.409	0.401	0.367
Pyramidal <a> slip (11-22) <-1-123>	0.415	0.424	0.408	0.411	0.413	0.405

3.2. Mechanical properties at room temperature

Fig. 5 describes the room temperature tensile properties of the rolled and ECAPed AZ31 sheets. The corresponding mechanical properties are listed in Table 2. It is especially noteworthy that route D provides a nearly isotropic stress-strain curve. This can be attributed to the combination of the shear deformation along the RD and TD between the successive passes. After the single pass, the effect of the shear deformation is evident from the improvement of ε_u in the RD (19.3%) compared to the rolled sheet (13.4%). Furthermore, the n-value in the RD is increased from 0.13 to 0.22. Hence, it is determined that high n-value enhances the ductility due to an increase in resistance to plastic instability. However, there is no enhancement of ε_u and n-value in the TD. On route D, ε_u in the RD, 45° and TD is 18.4, 20.6 and 17.2%, respectively. Compared to the single pass, ε_u in the RD is reduced slightly, but ε_u in the 45° and TD is enhanced by 6.7 and 17%, respectively. In this connection, the n-value in the TD is considerably increased from 0.15 to 0.21. Thus, ε_u in the TD is developed to a similar extent of the RD. Such a variation in the tensile properties can be explained by the microstructure and texture evolution as described above.

Suh et al. [14] reported that such an effect was evident from a monotonic increase in the fraction of the microstructure with high Schmid factors. The increase in Schmid factor for basal <a> slip and tension twinning was observed compared to the as-rolled condition [14]. On route D, this effect is evident from the decline in YS and the enhancement of ε_u and n-value particularly in the TD.

When the basal planes are distributed more broadly or inclined more along one direction than others, r-value increases as the angle between the texture-broadened direction and tensile direction increases [3]. In this respect, there is a distinct difference in r_{10} between the RD and TD (0.75 vs. 1.45) in the single pass. On route D, however, r_{10} in the RD, 45° and TD have a comparable value of 1 (refer to

Table 2). The Lankford coefficient close to 1 indicates an isotropic cross-sectional contraction, since the texture development on route D facilitates the thickness strain. For the above reasons, route D enables reducing the mechanical anisotropy of the ECAPed AZ31 sheet.

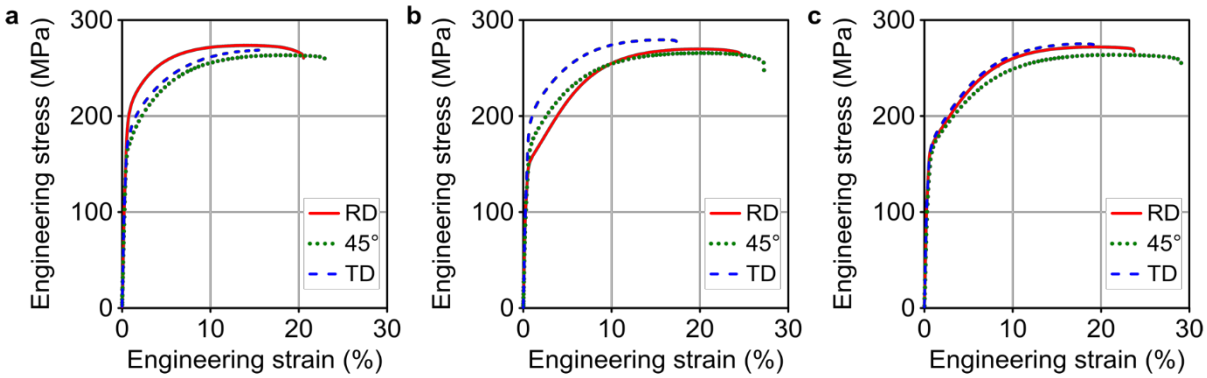

Fig. 5. Engineering stress-strain curves at room temperature of rolled and ECAPed AZ31 sheets: (a) as-rolled condition, (b) single pass, (c) route D.

Table 2 Tensile properties at room temperature of rolled and ECAPed AZ31 sheets (UTS: ultimate tensile strength).

	As-rolled			Single pass			Route D		
	RD	45°	TD	RD	45°	TD	RD	45°	TD
YS (MPa)	190	167	171	142	154	183	158	149	158
UTS (MPa)	275	264	269	268	265	280	271	264	276
ε_u (%)	13.4	17.4	14.8	19.3	19.3	15.0	18.4	20.6	17.2
r_{10} (-)	1.59	1.87	1.73	0.74	1.28	1.45	1.04	1.23	0.86
n-value (-)	0.13	0.17	0.17	0.22	0.19	0.15	0.20	0.22	0.20

3.3. Influence of texture on work hardening behavior

Fig. 6 presents the work hardening (WH) behavior of the rolled and ECAPed AZ31 sheets. The WH behavior in different processing conditions is remarkably distinct in terms of the WH rate ($\Theta = d\sigma / d\varepsilon_p$) as a function of $\sigma - \sigma_{0.2}$, where σ, $\sigma_{0.2}$ and ε_p are the true stress, 0.2% proof stress and true plastic strain, respectively. The term $\sigma - \sigma_{0.2}$ is related to the contribution of dislocation density to the flow stress [23]. The

rolled and ECAPed sheets show a steep hardening decrease with increasing the stress after elasto-plastic transition (stage I). In the WH plot, no stage II (Θ_{II} = constant) is observed and stage III is characterized by a linear decrease in Θ with increasing σ. This WH behavior in stage III is very similar to the well-known stage III in fcc polycrystals [23]. Such a behavior in stage III can be well described by a differential form of Voce equation [24] in terms of $\sigma - \sigma_{0.2}$ [25]:

$$\Theta = \Theta_0^{III}\left(1 - \frac{\sigma - \sigma_{0.2}}{\sigma_s}\right) \quad (1)$$

where Θ_0^{III} is a hardening limit extrapolated to $\sigma = \sigma_{0.2}$, and σ_s is a saturation stress extrapolated to $\Theta = 0$. The corresponding values of Θ_0^{III} and σ_s are listed in Table 2.

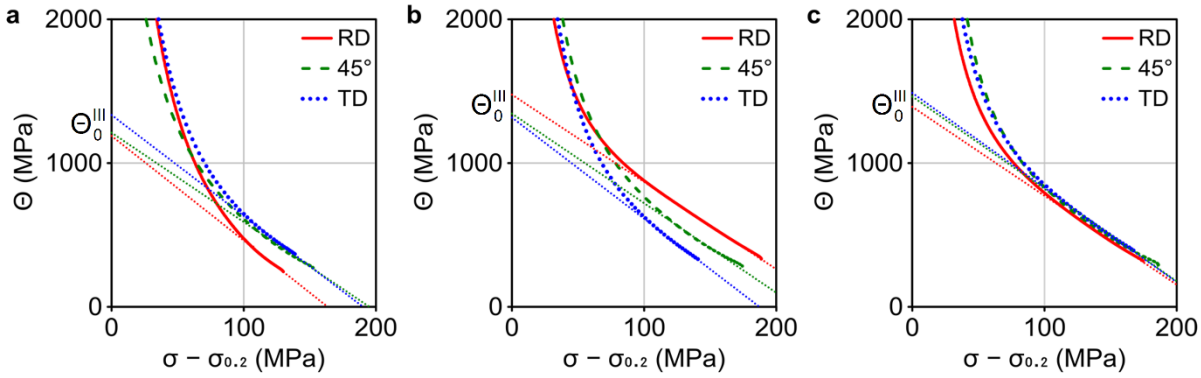

Fig. 6. Influence of texture on work hardening behavior of rolled and ECAPed AZ31 sheets in form of Θ vs. ($\sigma - \sigma_{0.2}$) plot: (a) as-rolled condition, (b) single pass, (c) route D.

Table 3 Extrapolated WH limit and saturation stress in stage III of rolled and ECAPed AZ31 sheets.

	As-rolled			Single pass			Route D		
	RD	45°	TD	RD	45°	TD	RD	45°	TD
Θ_0^{III}	1189	1212	1335	1477	1344	1317	1392	1463	1488
σ_s	164	195	190	243	216	187	225	228	226

The differences of the WH behavior in the rolled and ECAPed sheets can be attributed to texture effects. The rolled sheet exhibits a steep decline in Θ and the

lowest value in the RD, whereas the hardening behavior is similar in the TD and 45° (Fig. 6a). On the contrary, the ECAPed sheets exhibit higher Θ and slower drop than the rolled sheet. It can be considered that the shear deformation leads to a high WH and restrains dynamic recovery, which is related to the slope of the curves during stage III. In this way, the single pass shows the enhancement of Θ in the RD due to the inclination of the c-axis. However, there is a large difference in the WH behavior among three tensile directions and it results in high mechanical anisotropy (Fig. 6b). On the other hand, route D exhibits a comparable hardening behavior in all directions due to the shear deformation along the RD and TD (Fig. 6c).

Agnew et al. [26] reported that prismatic <a> slip exhibited a relative large activity compared with pyramidal <c+a> slip during in-plane extension at room temperature in AZ31 alloy. Cross-slip of <a> dislocations from basal to prismatic planes causes a decrease in Θ of the basal planes [23]. Dynamic recovery originates from this cross-slip of <a> dislocations and is related to softening behavior [23]. The slower decline in Θ of the ECAPed sheets indicates that the tilted c-axis, which is favorable for basal <a> slip, reduces the activation of prismatic <a> slip. As discussed above, the single pass and route D have the Schmid factor for prismatic <a> slip close to $m_{prismatic} \approx 0.36$ with respect to the orientation of the c-axis in the ECAPed samples. By contrast, the rolled sample shows $m_{prismatic} \approx 0.43$ in both tensile directions (refer to Table 1). Therefore, it can be inferred that the ECAPed texture inhibits cross-slip of <a> dislocations onto prismatic planes. Thus, dynamic recovery may be restrained by a texture that is favorable for basal <a> slip. This is in agreement with the hardening behavior of AM60 alloys processed by hot rolling and ECAP [23] and AZ31 sheets processed by differential speed rolling [27].

The activated {10-12} <10-11> twins are observed in the ECAPed AZ31 sheets with the texture tilting to the PD [14]. {10-12} twin boundaries with the reorientation of the

basal planes by ~86° can act as barriers to dislocation motion and become a source of work hardening [27]. The existing studies reported a similar observation on twin-induced work hardening [27-29]. Tension twinning induces an increase in the WH during deformation, leading to a larger ε_u [29]. Moreover, a complete reorientation of {10-12} tension twins can accommodate a theoretical maximum extension of 6.4% along the c-axis [19]. This effect can increase the uniform elongation in Mg alloys [30]. On route D, the shear deformation along the TD by ECAP induces the inclination of the c-axis as well as the activation of {10-12} tension twins in the TD. The restrained dynamic recovery and twin-induced work hardening result in the increase of the ε_u in the TD. As a result, route D provides a comparable WH behavior in three tensile directions, and hence allows an almost isotropic hardening of the ECAPed AZ31 sheet.

The hardening capacity (H_c) of a material can be described as a ratio of the UTS and YS and it is expressed as the following normalized parameter [31]:

$$H_C = \frac{UTS - YS}{YS} = \frac{UTS}{YS} - 1 \quad (2)$$

Fig. 7 depicts the direction-dependent H_c of the rolled and ECAPed sheets with respect to the n-value at room temperature. Since the UTS of both conditions are very comparable with each other, ECAPed sheets exhibit much higher H_c than the as-rolled condition due to lower YS and higher Θ. A significant enhancement of H_c is observed for the ECAPed samples in the PD. In conjunction with the WH behavior, H_c in the single pass is highest in the RD (0.89) and lowest in the TD (0.53), respectively. By contrast, route D has a comparable value of ~0.75 in three tensile directions. Especially, there is a close correspondence between the development of H_c and n-value. As mentioned above, the n-value also describes a hardening ability and high n-value promotes high uniform elongation due to an increase in resistance

to necking [32]. In a related development, the n-value of the ECAPed sheets shows a high degree of the directional dependence in accordance with the PD.

Such a different behavior is directly resulted from the texture effect. The rolled sample has a strong texture, which is not beneficial for basal <a> slip and requires higher initial stress to activate basal and non-basal slips. In the single pass, much lower H_c in the TD is observed due to the unfavorable distribution of the c-axis for basal slip compared to the RD. On the other hand, route D provides a comparable hardening ability because of a relative symmetrical distribution of the basal planes with the tilted c-axis.

Hardening capacity of a material is related to its YS and the following WH, which is attributed to dislocation strengthening effects [31]. According to the Hall-Petch relationship [33,34], grain refinement principally increases YS and hence reduces the H_c. It also reduces the difference of the flow resistance between grain boundary and interior, which in turn reduces H_c [35]. On the contrary, this present study shows that the texture modification during ECAP has a more dominant influence on the yield stresses than the grain refinement. This shows a good agreement with a decrease in YS of the conventional ECAPed bars of AZ31 [36] and AZ61 alloys [37].

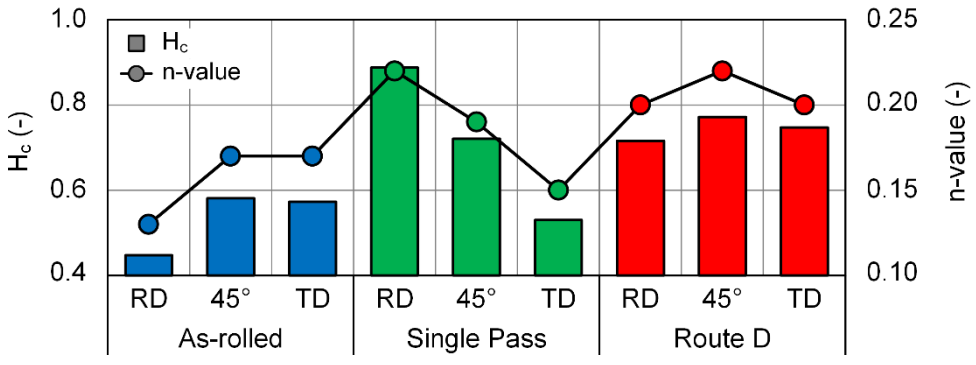

Fig. 7. Directional hardening capacity of rolled and ECAPed AZ31 sheets in consideration of n-value.

4. Conclusions

The present study investigated the effect of the modified processing route on the microstructure, texture and mechanical behavior at room temperature of the ECAPed AZ31 sheets. The main results from this study are summarized as follows:

1. On the new presented route D, the shear strain is imposed on the RD and subsequently on the TD with 90° rotation in the sheet plane. The change of the strain path is proven to be an effective way to tailor the texture of AZ31 sheets.
2. The microstructure of the ECAPed sheets is refined and a more homogenous microstructure with equiaxed grains develops through route D compared to the ECAPed sample in a single pass.
3. Shear deformation induced by ECAP makes a broad distribution of the basal planes along the PD. Grains with the tilted basal planes facilitates the activation of basal <a> slip and {10-12} <10-11> tension due to the increase in the Schmid factor.
4. Due to the increased activity of basal <a> slip and {10-12} tension twinning, the ECAPed sheets shows the decrease of YS and the enhancement of ε_u and n-value in the PD compared to the rolled sample.
5. Route D provides an almost isotropic hardening behavior at room temperature with the improved ε_u. It can be suggested that this is due to restrained dynamic recovery and twin-induced hardening behavior. In conjunction with work hardening behavior, route D exhibits a comparable H_c because of a relative symmetrical distribution of the basal planes with the tilted c-axis. Particularly, there is a close correspondence between the development of H_c and n-value. The current results also indicate that texture change has a more dominant influence on the mechanical properties rather than grain refinement in AZ31 Mg sheet.

Acknowledgements

This study is performed on the joint research project HO 2165/47-1 and LE 1395/6-1, which is financially supported by the Deutsche Forschungsgemeinschaft (DFG).

References

[1] K. Hantzsche, J. Bohlen, J. Wendt, K.U. Kainer, S. Yi, D. Letzig, Scripta Mater. 63 (2010) 725-730.

[2] A. Styczynski, Ch. Hartig, J. Bohlen, D. Letzig, Scripta Mater. 50 (2004) 943-947.

[3] B.C. Suh, M.S. Shim, K.S. Shin, N.J. Kim, Scripta Mater. 84-85 (2014) 1-6.

[4] S. Yi, J. Bohlen, F. Heinemann, D. Letzig, Acta Mater. 58 (2010) 592-605.

[5] R.B. Figueiredo, T.G. Langdon, J. Mater. Sci. 45 (2010) 4827-4836.

[6] S.R. Agnew, P. Mehrotra, T.M. Lillo, G.M. Stoica, P.K. Liaw, Acta Mater. 53 (2005) 3135-3146.

[7] T. Mukai, M. Yamanoi, H. Watanabe, K. Higashi, Scripta Mater. 45 (2001) 89-94.

[8] M. Furukawa, Z. Horita, T.G., Langdon, Mater. Sci. Eng. A 332 (2002) 97-109.

[9] R.B. Figueiredo, I.J. Beyerlein, A.P. Zhilyaev, T.G. Langdon, Mater. Sci. Eng. A 527 (2010) 1709-1718.

[10] R.B. Figueiredo, Z. Száraz, Z. Trojanová, P. Lukáč, T.G. Langdon, Scripta Mater. 63 (2010) 504-507.

[11] M. Furukawa, Y. Iwahashi, Z. Horita, M. Nemoto, T.G. Langdon, Mater. Sci. Eng. A 257 (1995) 328-332.

[12] W.J. Kim, S.I. Hong, Y.S. Kim, S.H. Min, H.T. Jeong, J.D. Lee, Acta Mater. 51 (2003) 3293-3307.

[13] J. Jufu, W. Ying, D. Zhiming, Q. Jianjun, S. Yi, L. Shouhing, J. Mater. Process. Technol. 210 (2010), 751-758.

[14] J. Suh, J. Victoria-Hernandez, D. Letzig, S. Yi, J. Bohlen, W. Volk, J. Mater. Process. Technol. 217 (2015) 286-293.

[15] Y. Iwahashi, J. Wang, Z. Horita, M. Nemoto, T.G. Langdon, Scripta Mater. 35 (1996) 143-146.

[16] J. Victoria-Hernandez, S. Yi, D. Letzig, D. Hernandez-Silva, J. Bohlen, Acta Mater. 61 (2013) 2179-2193.

[17] S.E. Ion, F.J. Humphreys, S.H. White, Acta Metall. 30 (1982) 1909-1919.

[18] C.S. Roberts, Magnesium and its Alloys, John Wiley, New York, 1960.

[19] P.G. Partridge, Int. Mater. Rev. 12 (1967) 169-194.

[20] M.H. Yoo, Metall. Trans. A. 12 (1981) 409-418.

[21] S. Yi, I. Schestakow, S. Zefferer, Mater Sci Eng A 516 (2009) 58-64

[22] E. Schmid, Kristallplastizität: Mit Besonderer Berücksichtigung der Metalle, Springer, Berlin, 1935

[23] J.A. del Valle, F. Carreno, O.A. Ruano, Acta Mater. 54 (2006) 4247-4259.

[24] E. Voce, J. Inst. Metals 74 (1948) 537-562.

[25] M. Karami, R. Mahmudi, Mater. Sci. Eng. A 607 (2014) 512-520.

[26] S.R. Agnew, C.N. Tomé, T.M. Brown, S.C. Vogel, Scripta Mater. 48 (2003) 1003-1008.

[27] X. Huang, K. Suzuki, A. Watazu, I. Shigematsu, N. Saito, Mater. Sci. Eng. A 488 (2008) 214-220.

[28] M.R. Barnett, Z. Keshavarz, A.G. Beer, D. Atwell, Acta Mater. 52 (2004) 5093.

[29] J. Bohlen, M.R. Nürnberg, J.W. Senn, D. Letzig, S.R. Agnew, Acta Mater. 55 (2007) 2101-2112.

[30] M.R. Barnett, Mater. Sci. Eng. A 464 (2007) 1-7.

[31] N. Afrin, D.L. Chen, X. Cao, M. Jahazi, Scripta Mater. 57 (2007) 1004-1007.

[32] S.R. Agnew, Ö. Duygulu, Int. J. Plast 21 (2005) 1161-1193.

[33] E.O. Hall, Proc. Phys. Soc. 64 (1951) 747-753.

[34] N.J. Petch, J. Iron Steel Inst. 173 (1953) 25-28.

[35] J. Luo, Z. Mei, W. Tian, Z. Wang, Mater. Sci. Eng. A 441 (2006) 282-290.

[36] H.K. Kim, W.J. Kim, Mater. Sci. Eng. A 385 (2004) 300-308.

[37] W.J. Kim, C.W. An, Y.S. Kim, S.I. Hong, Scripta Mater. 47 (2002) 39-44.